Journal of Atmospheric and Solar-Terrestrial Physics 163 (2017) 14–22

Contents lists available at ScienceDirect

Journal of Atmospheric and Solar-Terrestrial Physics

journal homepage: www.elsevier.com/locate/jastp

On statistical irregularity of stratospheric warming occurrence during northern winters

Elena N. Savenkova [a,**], Nikolai M. Gavrilov [a,*], Alexander I. Pogoreltsev [b,***]

[a] Atmospheric Physics Department, Saint-Petersburg State University, Saint-Petersburg, Russia
[b] Meteorological Forecast Department, Russian State Hydro-Meteorological University, Saint-Petersburg, Russia

ARTICLE INFO

Keywords:
Climatology
Stratospheric warming
Zonal-mean wind
Temperature
Planetary wave activity
Dynamical regime of the stratosphere

ABSTRACT

Statistical analysis of dates of warming events observed during the years 1981–2016 at different stratospheric altitudes reveals their non-uniform distributions during northern winter months with maxima at the beginning of January, at the end of January – beginning of February and at the end of February. Climatology of zonal-mean zonal wind, deviations of temperature from its winter-averaged values, and planetary wave (PW) characteristics at high and middle northern latitudes in the altitude range from the ground up to 60 km is studied using the database of meteorological reanalysis MERRA. Climatological temperature deviations averaged over the 60–90°N latitudinal bands reveal cooler and warmer layers descending due to seasonal changes during the polar night. PW amplitudes and upward Eliassen-Palm fluxes averaged over 36 years have periodical maxima with the main maximum at the beginning of January at altitudes 40–50 km. During the above-mentioned intervals of more frequent occurrence of stratospheric warming events, maxima of PW amplitudes and Eliassen-Palm fluxes, also minima of eastward winds in the high-latitude northern stratosphere have been found. Climatological intra-seasonal irregularities of stratospheric warming dates could indicate reiterating phases of stratospheric vacillations in different years.

1. Introduction

The coupling between the middle and lower atmosphere is extensively investigated on the base of observations and model simulations over several last decades.(e.g, Quiroz, 1975; Labitzke, 1977; Schoeberl, 1978). It is well known that sudden stratospheric warming (SSW) events are the clearest and strongest manifestation of the coupling of the stratosphere–troposphere system (Charlton and Polvani, 2007). Connected with SSWs circulation anomalies associated with strong or weak stratospheric polar vortex events can decent from the middle to the lower stratosphere where they persist, on average, for more than 2 months (e.g., Baldwin and Dunkerton, 2001) and produce substantial weather effects, for example, intense outbreaks of cold air in winter (e.g., Thompson et al., 2002). SSWs can also affect the circulation of the North Atlantic Ocean (Reichler et al., 2012), the effects of the El Niño - Southern Oscillation (ENSO) in Eurasia (e.g., Ineson and Scaife, 2009). They play an important role in stratospheric chemistry (e.g., Manney et al., 2003, 2005), transport of climate active gases and pollutants (Jiang et al., 2013; Butler et al., 2014), ozone variability in Arctic and Antarctic (e.g., Schoeberl and Hartmann, 1991). Evidences exist about SSW impacts on polar clouds in the troposphere (Kohma and Sato, 2014), on convective activity in the equatorial troposphere (e.g., Kodera, 2006), on dynamics of the mesosphere and formation of the stratopause (e.g., Siskind et al., 2007; Manney et al., 2005).

Since their first detection in 1952 (Scherhag, 1952), SSWs were extensively observed and categorized by the World Meteorological Organization. Gómez-Escolar et al. (2012) found an increase of SSW occurrence frequency in the post-satellite era from the analysis of the NCEP-NCAR and ERA-40 meteorological reanalysis datasets. The authors showed that SSWs tend to occur preferentially in January in the years 1958–1978, whereas they occur more often in December and at the end of February in years 1979–2002. Charlton and Polvani (2007) showed that typically SSWs occur in January–February with only a few SSWs occurring in November and December. Charlton and Polvani (2007) and Pawson and Naujokat (1999) demonstrated inter-annual SSW variability. They found a tendency toward reducing SSW activity during the mid-

* Corresponding author.
** Corresponding author.
*** Corresponding author.
E-mail addresses: savenkova.en@mail.ru (E.N. Savenkova), n.gavrilov@spbu.ru (N.M. Gavrilov), apogor@rshu.ru (A.I. Pogoreltsev).

http://dx.doi.org/10.1016/j.jastp.2017.06.007
Received 30 December 2016; Received in revised form 16 June 2017; Accepted 18 June 2017
Available online 20 June 2017

1990s, which was not continued at the beginning of the twenty-first century. Manney et al. (2005) analyzed the interval 1958–2004 and reported about highest SSW activity between the years 1998 and 2004. Pogoreltsev et al. (2015) demonstrated the important role of nonlinear interactions of the mean flow with stationary planetary waves in the SSW formation.

Butler et al. (2015) analyzed variety of existing SSW definitions using the NCEP-NCAR and ERA reanalysis data and provided tables of dates of all major SSWs observed in years 1958–2013. Gómez-Escolar et al. (2012) analyzed the frequency distribution of SSWs during 1957–2002 from the ERA-40 reanalysis data. They found different SSW numbers in different 10-day bins. These results raised an idea that the dates of major SSWs may have non-uniform distribution even at time scales of a few weeks during the winter months. To clarify this idea in this study, we performed a climatological analysis of atmospheric characteristics related to SSW developments.

Most of the mentioned above SSW climatology studies used the NCEP/ NCAR and ERA reanalysis datasets, which cover the longest period of observation in the stratosphere (since the year of 1958) with the upper boundary at the 10 hPa pressure level (approximately 30–35 km height). Recently, the Modern Era Retrospective-Analysis for Research and Applications (MERRA) database (Rienecker et al., 2011) and UK Met Office Assimilated Stratospheric Data (Swinbank and O'Neill, 1994) have been developed, which span the altitudes from the ground to 50 km (pressures up to 0.01 hPa). The analysis of 36-year (1981–2016) MERRA database (Rienecker et al., 2011) for altitudes up to 60 km was performed in the present study.

We estimated intra-seasonal distributions of dates of major and minor stratospheric warmings (SWs) as well as amplitudes and Eliassen-Palm (EP) fluxes of planetary wave (PW) components with zonal wavenumbers m ¼ 1 and m ¼ 2, EP-flux divergence, zonal-mean zonal wind and temperature deviations from its winter-mean values averaged over the 60–90°N latitudinal band at altitudes from the ground up to 60 km. These climatological data were compared with statistical distributions of observed dates of major SSWs given as supplement to the paper by Butler et al. (2015).

2. Methods of data analysis

The term "sudden stratospheric warming" is traditionally assigned to the abrupt increases in temperature associated with zonal wind reversals at the pressure level of 10 hPa (e.g., Butler et al., 2015). Fig. 1 represents an example of temperature deviation from the winter average value (Fig. 1a) and the zonal wind (Fig. 1b) for winter months of the year 1982 obtained from the MERRA database at high latitudes. One can see sharp increase in polar stratospheric temperature in the second part of January and corresponding reversal of the zonal wind direction. However, this reversal exists at altitudes above 10 hPa level and, strictly speaking, this event can not be treated as SSW according to the WMO rules. To distinguish such events at higher stratospheric levels from traditionally discussed SSW events, we call them here as "high stratospheric warming (HSW) events".

In Fig. 1b the zero zonal wind contour appear first at altitude about 50 km on January 23. This altitude and date are considered here as the date and location of the HSW. At altitudes below 40 km the zonal wind reversal occurs 1–2 days later than that at 50 km level in Fig. 1b. Dates and heights of all HSWs obtained from the MERRA database for years 1981–2016 are given in the Supplementary Table 2 to the present paper. Fig. 1a shows the second substantial temperature increase (up to 20 K) at the end of February. One can see respective decrease in the zonal wind in Fig. 1b, however the wind does not drop below zero. One can treat such events as "minor HSW". In the Supplementary Table 2, we included such minor SSWs, for which the zonal wind drops below 10 m/s at latitude 62.5°N and mark them as "0 < u < 10". The date and altitude of minor HSW are determined using the contour of lowest zonal wind (10 m/s for Fig. 1b at the end of February).

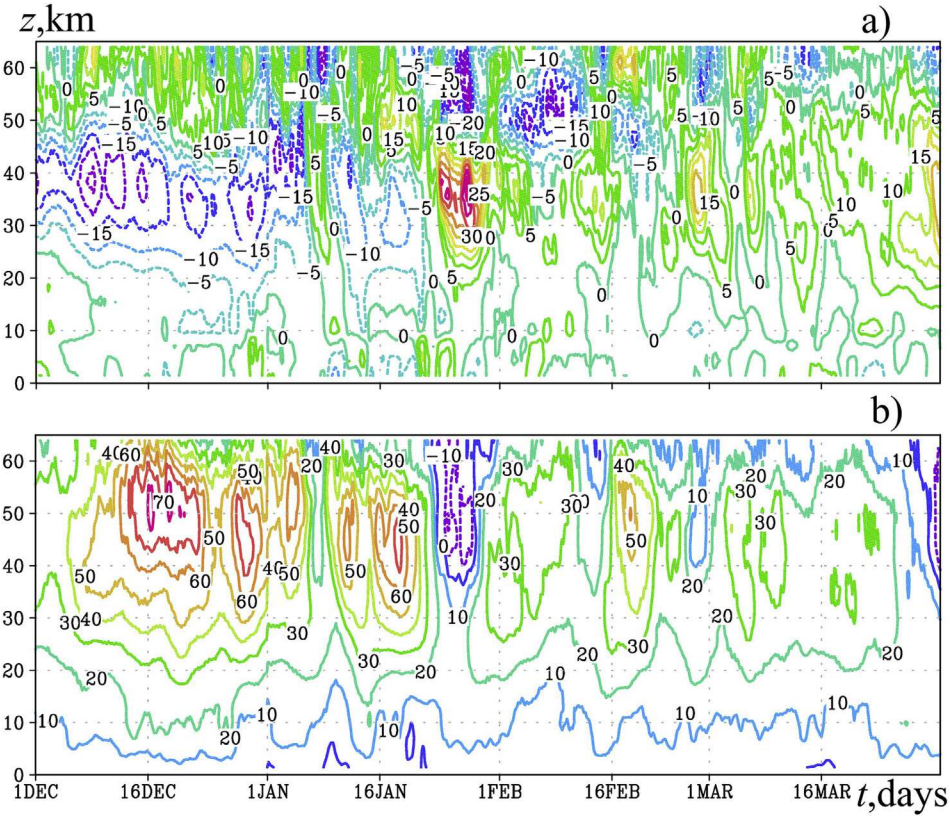

Fig. 1. Example of temperature deviation in K from the winter average value at latitude 87.5°N (a) and zonal velocity in m/s at latitude 62.5°N (b) for winter months of year 1982 obtained from the MERRA database.

Among atmospheric characteristics responsible for SW formation, the amplitude of stationary PWs with zonal wave number m ¼ 1 and m ¼ 2, vertical components of EP-flux, also the zonal-mean zonal wind and temperature deviations averaged over the 60–90°N latitudinal band have been considered. To obtain parameters of PWs, all meteorological variables have been decomposed using the Fourier analysis into the zonal-mean values and a superposition of harmonics with zonal wave numbers m ¼ 1–4 (called as PW1–PW4 below).

Most of studies devoted to the PW propagation used the three main diagnostic tools: numerical general circulation modeling, analysing observations to estimate the EP-flux and its divergence, and analysing the atmospheric refractive index for PW modes. The EP-flux and its

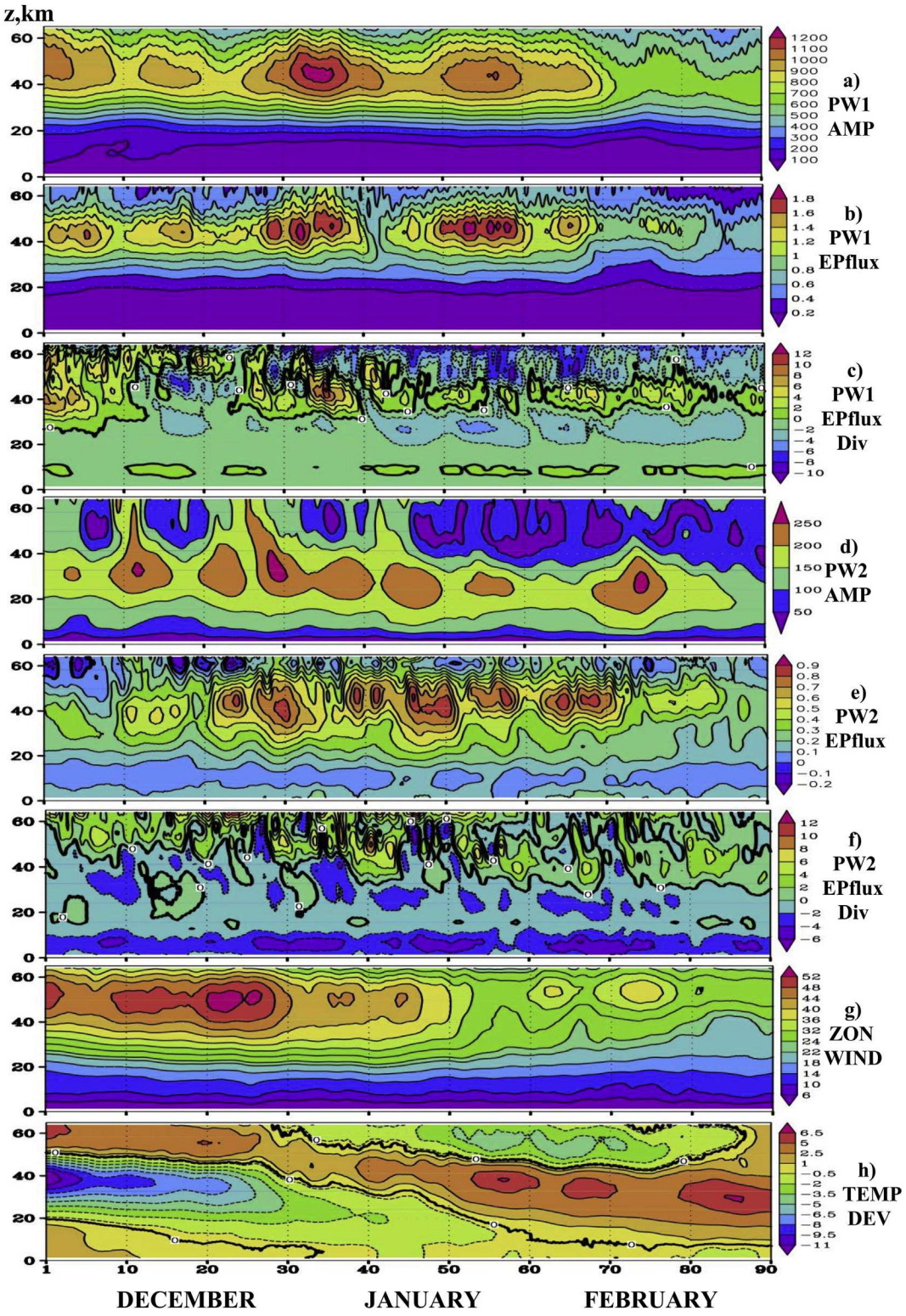

Fig. 2. Averaged PW1 geopotential height amplitude in gpm – a; PW1 vertical component of EP-flux in kg m^{-1} s^{-2} – b; PW1 divergence of EP-flux in kg m^{-2} s^{-2} – c; PW2 geopotential height amplitude in gpm – d; PW2 vertical component of EP-flux –e; PW2 divergence of EP-flux – f; zonal-mean zonal wind in m/s – g; deviations of temperature from its winter-mean values in K averaged over 60–90N latitudinal band – h, obtained from MERRA data for years 1981–2016. Thick black lines denote zero contours.

divergence (Andrews et al., 1987) represent the wave activity and the eddy forcing, respectively. Theoretically, PWs tend to avoid regions where zonal winds are easterly, or westerly and exceeding the critical Rossby velocity as it is shown by many papers (e.g., Charney and Drazin, 1961). They are attracted towards regions where the values of the refractive index squared are positive (Andrews et al., 1987). It is shown in many papers that the refractive index is a useful diagnostic tool for vertical and meridional PW propagation.

Analyses of SW formation mechanisms often include considerations of the EP-fluxes to diagnose the eddy forcing (e.g., Andrews et al., 1987; Andrews and McIntyre, 1976). The vector of the EP flux represents the zonal-mean direction of wave activity propagation in the meridional plane. Meridional and vertical EP-flux components include the eddy momentum and heat fluxes. In this study, climatological values of the vertical EP-flux component F_z for PW modes with zonal wave numbers m ¼ 1 and m ¼ 2 have been estimated using the conventional formula (e.g. Inoue et al., 2011):

$$F_z = \rho_0 a \cos\varphi \left\{ f \frac{1}{a\cos\varphi} \frac{\partial}{\partial\varphi}(\bar{u}\cos\varphi) - \frac{\overline{v'\theta'}}{\bar{\theta}_z} \right\} - \overline{w'u'}, \quad (1)$$

where a and f are the mean Earth's radius and the Coriolis parameter, respectively; ρ_0 is the background density; φ is latitude; u, v, w are zonal, meridional and vertical wind components, respectively; θ is potential temperature; overbars and primes denote the zonal-mean values and deviations from them, respectively. Divergences of EP-flux showing wave drag of the mean flow and the rate of change of PW wave-activity (Andrews et al., 1987) were also calculated for PW modes with zonal wave numbers m ¼ 1 and m ¼ 2.

To identify HSWs we generally followed their definitions by Charlton and Polvani (2007), but the reverse of zonal wind have been checked at higher than 10 hPa pressure level altitudes up to 60 km.

3. Results

The described above methods were used for determination of HSW related characteristics from the 36-year (1981–2016) MERRA database (Rienecker et al., 2011) for altitudes up to 60 km.

3.1. HSW date statistics

Fig. 2 shows satellite amplitudes, vertical components and divergences of EP-flux for PW1 and PW2, zonal-mean zonal wind and temperature deviation from its winter-mean values averaged for each day of December–February at middle and high northern latitudes, respectively, over the entire analyzed interval using the MERRA database. Fig. 2h demonstrates temperature deviations from its seasonal means, averaged over the 60–90°N latitudinal bands. One can see descending cooler and warmer layers, which reflect seasonal changes of temperature in the troposphere–stratosphere caused by decreasing the Earth's surface temperature to a minimum in January–February and by seasonal changes in radiation influxes and circulation in the stratosphere during polar nights. Examinations of height-latitude distributions of monthly-mean temperatures at altitudes 5–35 km from CHAMP low-orbit GPS satellite data (Gavrilov, 2007) show strongest temperature minima above altitude 30 km near the North Pole in November–December. Then these minima become lesser and shift downwards in accordance with Fig. 2h.

Besides seasonal changes, one can see localized temperature maxima in Fig. 2h inside the warmer layer. One of the reasons for these maxima could be the cumulative effect of SSWs and HSWs occurring in the winter stratosphere. The existence of several local temperature maxima in Fig. 2h allows assuming inhomogeneous distributions of HSW dates with higher occurrence frequencies on certain days during winter. Cross-sections of these temperature maxima at altitude about 35 km may correspond to more frequent occurrence of major and minor SSWs determined with the standard WMO rules at the pressure level of 10 hPa. Besides that, the local temperature maxima in Fig. 2h expand to other stratospheric altitudes, where they can indicate similar warming events, which we call as HSWs here (see above).

To study such possibilities we obtained the dates of major and minor SSWs and HSWs at different altitudes using the MERRA (years 1981–2016) meteorological reanalysis database (see Section 2). Then we calculated numbers of all SW dates from Supplementary Table 2 within consecutive 10-day intervals represented in the first row of Table 1. HSWs were detected at different stratospheric altitudes between 30 and 60 km in almost every winter season (except year 1988) between years 1981–2016 (see Supplementary Table 2 and Pogoreltsev et al., 2014). The numbers of major SSWs found by Butler et al. (2015) from NCAR/NCEP data during the years 1958–1980 are added to the second row of Table 1. The third row of Table 1 gives sums of HSW and SSW numbers from the first two rows for respective bins. The last row in Table 1 shows the number of SSWs obtained from MERRA data for years 1981–2016 using their determination at the pressure level of 10 hPa (e.g., Charlton and Polvani, 2007). These SSW dates from MERRA database are generally the same as those obtained from NCAR/NCEP and MERRA data for years 1981–2013 by Butler et al. (2017).

To verify the hypothesis about non-uniform distribution of HSWþ SSW dates we applied the statistical chi-square test (e.g. Rice, 2006) to the first and third rows of Table 1. For each row the value $\chi^2 = \sum_{i=1}^{M} (n_i - n_0)^2 / n_0$ was calculated, where M is the number of bins in Table 1, n_i is the HSW number in i-th bin, $n_0 = N/M$ is expected number for the homogeneous distribution, N is the total number of HSWs in M analyzed sells of Table 1. For the first and third rows of Table 1 M ¼ 9 and χ^2 ¼ 13.7 and χ^2 ¼ 16.2, respectively. According to the χ^2-table for M − 1 ¼ 8 freedom degrees (e.g., PennState, 2016), these χ^2 values correspond to the probability of uniform statistical distribution below 0.09 and 0.04 for the first and third rows, respectively. This proves the statistical irregularity of HSW occurrence dates versus time during winter.

Numbers of registered HSWs in the third row of Table 1 have local maxima at the beginning of January, at the end of January – beginning of February and at the end of February. To make further verifications of these maxima, we performed three additional chi-square tests of inhomogeneity of HSW date distributions within 3 bins of the third row of Table 1 that contain nearby maxima and minima of HSW numbers. For specified above three local maxima of HSWþ SSW occurrence M ¼ 3 and χ^2 ¼ 4.2, 6.1, 3.2, respectively. The χ^2-table for M − 1 ¼ 2 freedom degrees gives the probabilities of homogeneous statistical distributions in the vicinity of the mentioned three maxima less than 0.1, 0.05 and 0.2, respectively. This confirms substantial statistical significance of the local maxima of HSWþ SSW numbers in the third row of Table 1.

Specified above intervals of maximum numbers of HSWþ SSW events in the third row of Table 1 (the beginning of January, the end of January – beginning of February and the end of February) correspond to the

Table 1
Numbers of HSW and SSW events registered in consecutive 10-day intervals from the meteorological reanalysis datasets MERRA and from NCEP/NCAR (obtained by Butler et al., 2015).

Month	N	December			January			February		
Days from Dec. 1		1–10	11–20	21–30	31–40	41–50	51–60	61–70	71–80	81–90
MERRA, HSWþ SSW 1981–2016	63	4	3	4	10	4	13	9	7	9
NCAR/NCEP, SSW 1958–1980	20	3	2	1	3	3	5	0	0	3
Total HSWþ SSW 1958–2016	83	7	5	5	13	7	18	9	7	12
MERRA, SSW 1981–2016	19	2	1	1	3	1	3	1	2	5

locations of temperature maxima in Fig. 2h and confirm that these temperature maxima can be produced by more frequent HSW events during these intervals.

3.2. Average HSW related characteristics

To clarify the reasons for described above irregularities of the statistical distribution of HSW dates, the climatological variability of atmospheric characteristics related to the HSW formation has been analyzed.

Fig. 2a, d demonstrate, respectively, the time-altitude cross-sections of PW1 and PW2 amplitudes at 62°N latitude averaged over the last 36-years of MERRA dataset (see above). Fig. 2a shows quasi-periodical vacillations of PW1 with amplitude maxima every 15–20 days (the main maximum exists at the beginning of January at altitudes 40–50 km). These maxima correspond to respective maxima of the vertical EP-flux in Fig. 2b. These fluxes are almost everywhere positive reflecting upward propagation of the wave activity from the wave source regions in the lower atmosphere. Positive vertical component of EP-flux in Fig. 2b corresponds to the northward direction of the zonal-average meridional heat flux produced by PW1. This confirms existing views (e.g., Holton and Mass, 1976) about heating of the polar stratosphere by PWs with consequent decreasing eastward Polar Vortex velocities and thus contributing to HSW developments.

Maxima of the multiyear average PW1 EP-flux in Fig. 2b correspond to PW1 amplitude maxima in Fig. 2a. They occur generally after respective local maxima of multiyear average zonal winds shown in Fig. 2g. A reason for quasi-periodical variations of the mean wind with periods of 1–4 weeks could be vacillations caused by changes in the conditions of PW propagation and by nonlinear interactions of PWs with the mean flow (e.g. Holton and Mass, 1976). Intensities and durations of these vacillations may change from year to year. At entirely random distribution of vacillation phases, one should anticipate complete disappearing local maxima and minima in Fig. 2a, b and g. Survival of multiyear average local maxima in Fig. 2 could indicate the vacillation phase reiteration in different years.

Fig. 2d and 2e reveal multiyear average PW2 amplitudes and vertical EP-flux components. Fig. 2e contains local regions of negative (downward) vertical PW2 EP-flux components. They may be caused by reflections of PW2 propagating from below and/or by PW2 mode generation in the middle atmosphere. Relative dimensions of regions with negative EP-fluxes in Fig. 2e are smaller than those for positive EP-fluxes. Negative vertical EP-fluxes correspond to southward wave heat fluxes and to additional cooling of the middle atmosphere near the North Pole.

The main PW2 amplitude maxima in Fig. 2d are visible at altitudes about 30 km, which are substantially lower, than the altitudes of PW1 maxima at 40–50 km in Fig. 2a. A reason could be stronger influence of the mean wind on the PW2 refractive index, which could prevent PW2 propagation into the region of strong eastward winds. Numerical simulations of height-latitude distributions of different PW amplitudes by Gavrilov et al. (2015) revealed amplitude maxima of stationary PW2 modes at altitudes 30–40 km at high latitudes of the winter Northern Hemisphere.

Climatological PW2 maxima in Fig. 2d are repeating with time intervals about 9–10 days. Numerical study by Robinson. (1985) showed vacillations with anti-phase changes of PW1 and PW2 amplitudes in the stratosphere. In Fig. 2a, PW2 maxima often occur in between PW1 maxima, which are consistent with simulations by Robinson. (1985) and allow assuming energy exchanges between PW1 and PW2 modes due to nonlinear wave interactions.

For further understanding of PW1 and PW2 amplitude behavior, Fig. 2a and 2f show divergences of EP-fluxes, which represent wave drag of the mean flow and changes in the wave action of respective PW modes (Andrews et al., 1987). Fig. 2c reveals maxima of multiyear average PW1 EP-flux divergence at altitudes 30–50 km with higher positive divergences during PW1 amplitude maxima shown in Fig. 2a. Positive EP-flux divergence corresponds to the acceleration of the mean flow and decreasing PW1 wave-action, which is consistent with the mechanism of stratospheric vacillations (e.g. Holton and Mass, 1976). EP-flux divergences for PW2 in Fig. 2f are mainly negative at altitudes 20–40 km and positive at lower and higher altitudes. Negative EP-flux divergences match to increases in PW2 wave-activity and amplitudes at altitudes 30–40 km seen in Fig. 2d. For some PW2 amplitude maxima in Fig. 2e, their anti-phase behavior with PW1 maxima in Fig. 2a is less clear. This may be connected with differences between heights of the main PW1 (40–50 km) and PW2 (30–40 km) maxima and with other mechanisms influencing PW propagation in the middle atmosphere.

Climatological average zonal-mean eastward winds in Fig. 2g are larger than 30 m/s (with maxima up to 55 m/s) at altitudes above 30 km before the end of January and become weaker than 30 m/s after January 20–25. This coincides with time intervals, when the lower boundary of warmer zone in Fig. 2f crosses altitudes 25–30 km and the polar stratosphere becomes warmer. At the middle of February, the polar stratosphere becomes cooler at altitudes 40–50 km (see Fig. 2h) and the average zonal wind there becomes again stronger for a week or two in Fig. 2g.

Comparisons of the intervals of more frequent HSW occurrence in Table 1 (the beginning of January, the end of January – beginning of February and the end of February) with Fig. 1a and 1b detect local maxima of PW1 amplitudes and EP-fluxes during these intervals (with smaller maxima magnitudes for the last interval due to seasonal changes). All three mentioned time intervals of increased HSW occurrence correspond to decreases in the climatological eastward wind velocity in Fig. 2g. Therefore, more frequent HSW occurrence during the mentioned time intervals could be explained by the reiteration of PW vacillation phases in different years discussed above.

Consideration of the last row in Table 1 and the SSW database by Butler et al. (2017) shows many years, when the MERRA data do not reveal any existence of SSWs at the 10 mb pressure level. Figs. 3 and 4 represent data similar to Fig. 2 but for years with SSWs (1980, 82, 84, 85, 87–89, 99, 2001, 02, 03, 04, 06–10, 13) and without SSWs (1981, 83, 86, 90–98, 2000, 05, 11, 12, 14–16), respectively. Comparison of Figs. 3h and 4h show cooler polar stratosphere at altitudes 30–50 km in non-SSW years in December. This leads to higher westward velocity of Polar Vortex in the beginning of winter in Fig. 4g compared to Fig. 3g, which suppress PW propagation and hold smaller PW1 and PW2 amplitudes up to the end of December in non-SSW years (compare Fig. 4a, d and 3a, d). Therefore, stratospheric vacillations between PW amplitudes and the mean wind start later in non-SSW years in Fig. 4a, d, g and substantial temperature variations occur at higher than 10 hP A pressure level altitudes in non-SSW years (Fig. 4h) than those in Fig. 3h for years with SSW. Fig. 3h reveals smaller temperature variability below 40 km altitudes until the end of January and in the first part of February in years with SSW. The differences may be caused by smaller PW1 amplitudes in these intervals during years with SSWs in Fig. 3a compared to Fig. 4a for years without SSW events. This may explain smaller numbers of SSW events during mentioned above intervals as registered from the MERRA data in the last row of Table 1 compared with respective numbers of HSWþ SSW in the first row in Table 1.

Analysis of differences between years with and without SSWs observed at 10 hPa pressure level is not the primary goal of the present paper. Further studies of these differences are required.

4. Discussion

It is known that PWs are mainly controlled by the structure of zonal mean wind and its vertical shear (Andrews et al., 1987). In turn, PWs could strongly influence the mean flow according to the wave-mean flow interaction theorem (Andrews et al., 1987). The mean zonal wind can change the refractivity index for atmospheric waves and thus influence EP-fluxes and PW1 amplitudes. Furthermore, PW1 can drag the mean

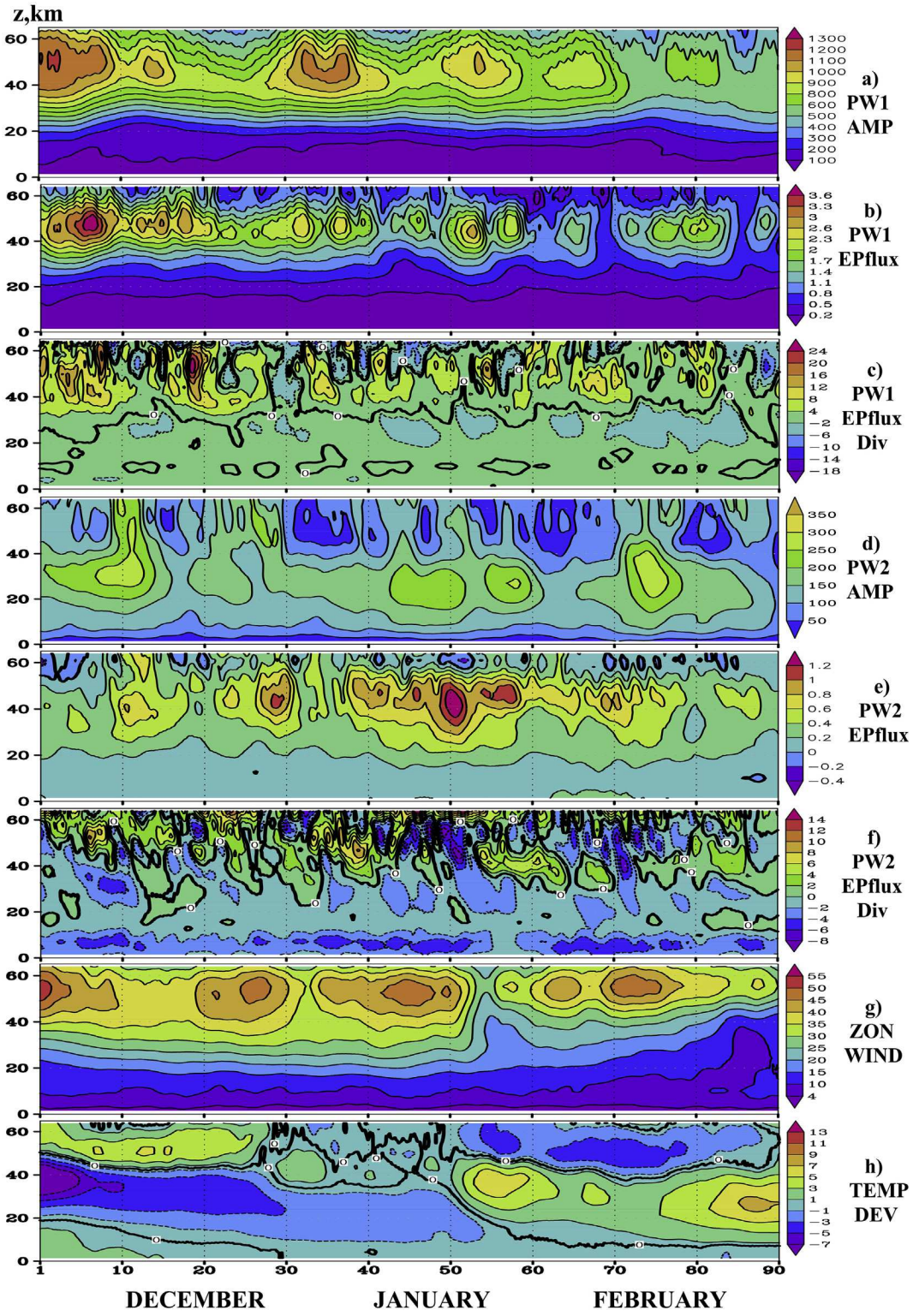

Fig. 3. Same as Fig. 1, but for the years with SSW: 1980, 82, 84, 85, 87–89, 99, 2001, 02, 03, 04, 06–10, 13.

flow triggering energy transfer from the mean flow to the waves. In addition, positive vertical components of EP-flux in Fig. 2b correspond to PW1 heat fluxes directed to the North Pole and to additional heating of polar regions by waves, which can weakening the polar vortex and diminish eastward velocity. Such wave-mean flow interactions can produce vacillations with quasi-periodical maxima and minima of the zonal velocity and PW1 amplitudes seen in Fig. 1a and 1e.

During winter time in the Northern Hemisphere, PWs generated in the troposphere by the topography and diabatic heating will propagate upwards to the stratosphere, where zonal mean zonal winds are westerly and do not exceed the critical Rossby velocity (Andrews et al., 1987). The critical Rossby velocity depends on the wave number and latitude, implying that only ultra-long waves have the possibility to propagate to the stratosphere at middle and high latitudes (Matsuno, 1970).

Fig. 1a and 1d show that PW1 can propagate in the upper stratosphere while PW2 has maxima at lower altitudes. According to the atmospheric

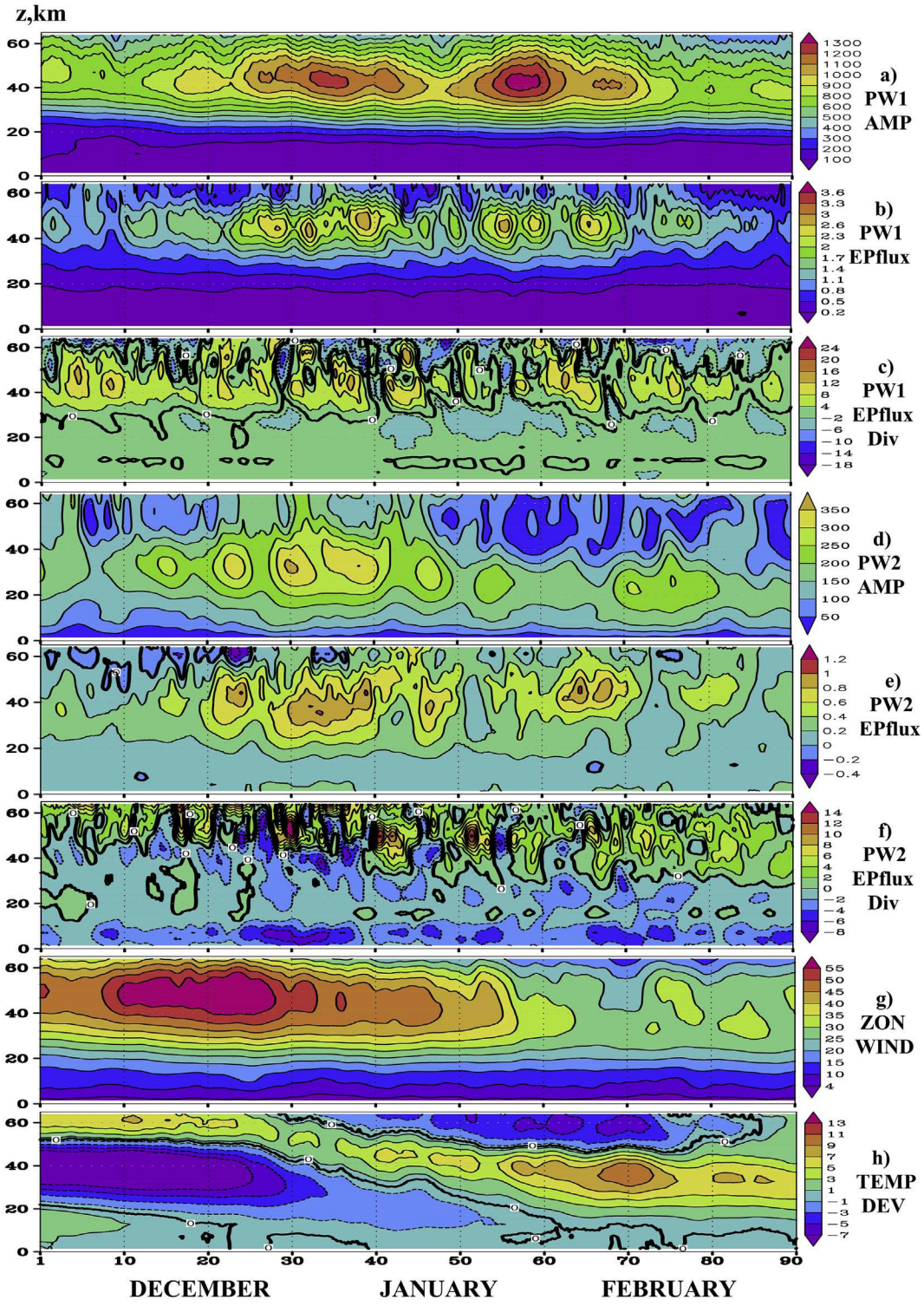

Fig. 4. Same as Fig. 1, but for the years without SSW: 1981, 83, 86, 90–98, 2000, 05, 11, 12, 14–16.

wave theory, PWs can propagate in waveguides, where the PW refractivity index squared is positive (e.g. Andrews et al., 1987). Formulae for the PW refractivity index (e.g. Andrews et al., 1987; Albers et al., 2013) show that PW1 is able to propagate in stronger westerly mean flow, than PW2. In addition, PW1 mode may accelerate or decelerate the mean flow depending on PW1 phases (see positive and negative EP-flux divergences in Fig. 2c). This may change conditions of PW2 propagation and PW2-mean flow interactions (see Fig. 2f). The majority of PW2 amplitude maxima in Fig. 2d are located in between of PW1 amplitude maxima shown in Fig. 2a.

EP-flux divergences for PW2 in Fig. 2f are mainly positive above altitudes 40 km, which corresponds to accelerations of the mean flow and decreasing PW2 wave-activity. This could explain localizations of PW2 amplitude maxima in Fig. 2d mostly at altitudes 20–40 km, where EP-flux divergences are manly negative in Fig. 2f. However, negative PW2 EP-flux divergences can sometimes exist at altitudes above 40 km (see Fig. 2f), which could enhance PW2 amplitudes at high altitudes in Fig. 2d.

Charlton and Polvani (2007) made statistical analysis of dates of 28 major SSWs in the years 1958–2002 obtained from NCAR/NCEP and ERA-40 datasets. They found maximum of SSW occurrence in January and little bit smaller SSW number in February. Calculating total HSW numbers in the third row of Table 1 correspond to these results. Unfortunately, low SSW numbers obtained by Charlton and Polvani (2007) do not allow getting detailed intra-seasonal distributions of SSW dates as we do for HSWs in the present paper. Gómez-Escolar et al. (2012) analyzed intra-seasonal variations of SSW numbers observed during the years 1958–2002. They found maxima of SSW numbers during northern winter similar to those shown in Table 1 and their changes in the years 1958–1979 and 1980–2002. Our study may be considered as continuation of these studies for wider altitude range (0–60 km) using the recent MERRA dataset and involving climatology of HSW related atmospheric characteristics.

Good agreement between changes in HSW numbers in Table 1 and independently obtained respective variations of multiyear average HSW characteristics in Fig. 2 could give additional evidences of intra-seasonal statistical irregularities of HSW date distribution. The maximum numbers of HSWþ SSW events in the third row of Table 1 are observed at the beginning of January, the end of January – beginning of February and at the end of February. It was mentioned above that quasi-periodical variations of the mean wind and PW1 and PW2 amplitudes with periods of 1–4 weeks could be stratospheric vacillations (e.g. Holton and Mass, 1976; Robinson, 1985). In case of completely random phases of these vacillations in different years, one should expect homogeneous distributions of multi-year average dynamical characteristics and HSW numbers during winter. The existence of pronounced local maxima in Fig. 2 and Table 1 could reflect reiterations of certain phases of stratospheric vacillations in different years.

5. Conclusions

In this study, the statistical distributions of SSW and HSW dates and atmospheric parameters related to their developments are analyzed using the 36-year (1981–2016) daily meteorological MERRA dataset and the 57-year (1958–2013) NCAR/NCEP reanalysis data. Statistical distribution of HSW occurrence numbers demonstrates irregular behavior with maxima of the HSW occurrence at the beginning of January, at the end of January – beginning of February and at the end of February.

Climatological atmospheric characteristics related to HSW formation at altitudes up to 60 km have been studied from the MERRA database. We analyzed multiyear average amplitudes, EP-fluxes and their divergences for PW components with zonal wave numbers m ¼ 1 and m ¼ 2, also the zonal-mean zonal wind and deviations of temperature from its winter-mean values at high northern latitudes.

Multiyear average temperature deviations reveal descending cooler and warmer layers due to seasonal changes during polar night. Multiyear PW1 amplitudes and upward vertical components of EP-flux have quasi-periodical maxima with the main maximum at the beginning of January in the altitude range 40–50 km. The main climatological maxima of PW2 amplitudes and upward EP-fluxes are located at lower altitudes about 30 km. During intervals of HSW occurrence maxima at the beginning of January, at the end of January – beginning of February and at the end of February, climatological maxima of temperature deviations, minima of eastward winds, also maxima of PW1 amplitudes and EP-fluxes exist. Years without SSW events demonstrate cooler polar stratosphere, higher velocity of Polar Vortex and smaller PW1 and PW2 amplitudes in the beginning of winter and later beginning of stratospheric vacillations.

Further studies are required to understand whether these long-term differences observed during the last decades reflect stable trends or temporal variability in the atmospheric climate system.

Funding

This work was supported by the Russian Foundation for Basic Research [grant number 17-05-00458a].

Acknowledgements

We are grateful to NASA for access to the MERRA data.

Appendix A. Supplementary data

Supplementary data related to this article can be found at http://dx.doi.org/10.1016/j.jastp.2017.06.007.

References

Albers, J.R., McCormack, J.P., Nathan, T.R., 2013. Stratospheric ozone and the morphology of the Northern Hemisphere planetary waveguide. J. Geophys. Res. Atmos. 118, 563–576. http://dx.doi.org/10.1029/2012JD017937.

Andrews, D.G., McIntyre, M.E., 1976. Planetary waves in horizontal and vertical shear: the generalized Eliassen-Palm relation and the mean zonal acceleration. J. Atoms. Sci. 33, 2031–2048.

Andrews, D.G., Holton, J.R., Leovy, C.B., 1987. Middle Atmosphere Dynamics. Elsevier, New York.

Baldwin, M.P., Dunkerton, T.J., 2001. Stratospheric harbingers of anomalous weather regimes. Science 294, 581–584. http://dx.doi.org/10.1126/science.1063315.

Butler, A.H., Polvani, L.M., Deser, C., 2014. Separating the stratospheric and tropospheric pathways of El Niño–Southern oscillation teleconnections. Environ. Res. Lett. 9, 024014 http://dx.doi.org/10.1088/1748-9326/9/2/024014.

Butler, A., Seidel, D., Hardiman, S., et al., 2015. Defining sudden stratospheric warmings. Bull. Amer. Meteorol. Soc. http://dx.doi.org/10.1175/BAMS-D-13-00173.1. Supplement doi 10.1175/BAMS-D-13-00173.2.

Butler, A.H., Sjoberg, J.P., Seidel, D.J., Rosenlof, K.H., 2017. A sudden stratospheric warming compendium. Earth Syst. Sci. Data 9, 63–76. http://dx.doi.org/10.5194/essd-9-63-2017.

Charlton, A.J., Polvani, L.M., 2007. A new look at stratospheric sudden warmings. Part I: climatology and modeling benchmarks. J. Clim. 20, 449–469.

Charney, J.G., Drazin, P.G., 1961. Propagation of planetary-scale disturbances from the lower into the upper atmosphere. J. Geophys. Res. 66, 83–109.

Gavrilov, N.M., 2007. Monthly Height-latitude Distributions of Temperature Mesoscale Variances at Altitudes 0-35 Km in Years 2001-2005 from CHAMP GPS Satellite Data. http://dx.doi.org/10.13140/RG.2.1.3214.7046. ResearchGate Dataset.

Gavrilov, N.M., Koval, A.V., Pogoreltsev, A.I., Savenkova, E.N., 2015. Simulating influences of QBO phases and orographic gravity wave forcing on planetary waves in the middle atmosphere. Earth Planets Space 67, 86. http://dx.doi.org/10.1186/s40623-015-0259-2.

Gómez-Escolar, M., Fueglistaler, S., Calvo, N., Barriopedro, D., 2012. Changes in polar stratospheric temperature climatology in relation to stratospheric sudden warming occurrence. Geophys. Res. Lett. 39, L22802 http://dx.doi.org/10.1029/2012GL053632.

Holton, J.R., Mass, C., 1976. Stratospheric vacillation cycles. J. Atmos. Sci. 33, 2218–2225.

Ineson, S., Scaife, A.A., 2009. The role of the stratosphere in the European climate response to El Niño. Natl. Geosci. 2, 32–36. http://dx.doi.org/10.1038/ngeo381.

Inoue, M., Takahashi, M., Naoe, H., 2011. Relationship between the stratospheric quasi-biennial oscillation and tropospheric circulation in northern autumn. J. Geophys. Res. 116, D24115 http://dx.doi.org/10.1029/2011JD016040.

Jiang, X., Wang, J., Olsen, E.T., Pagano, T., et al., 2013. Influence of stratospheric sudden warming on AIRS mid-tropospheric CO2. J. Atmos. Sci. 70, 2566–2573. http://dx.doi.org/10.1175/JAS-D-13-064.1.

Kodera, K., 2006. Influence of stratospheric sudden warming on the equatorial troposphere. Geophys. Res. Lett. 33, L06804 http://dx.doi.org/10.1029/2005GL024510.

Kohma, M., Sato, K., 2014. Variability of upper tropospheric clouds in the polar region during stratospheric sudden warmings. J. Geophys. Res. Atmos. 119 http://dx.doi.org/10.1002/2014JD021746, 1010010113.

Labitzke, K., 1977. Interannual variability of the winter stratosphere in the Northern Hemisphere. Mon. Weather Rev. 105 (6), 762–770. http://dx.doi.org/10.1175/1520-0493(1977)105<0762:IVOTWS>2.0.CO;2.

Manney, G.L., Sabutis, J.L., Pawson, S., et al., 2003. Lower stratospheric temperature differences between meteorological analyses in two cold Arctic winters and their impact on polar processing studies. J. Geophys. Res. Atmos. 108, 8328. http://dx.doi.org/10.1029/2001JD001149.

Manney, G.L., Kruger, K., Sabutis, J.L., et al., 2005. The remarkable 2003–2004 winter and other recent warm winters in the Arctic stratosphere since the late 1990s. J. Geophys. Res. 110, D04107 http://dx.doi.org/10.1029/2004JD005367.

Matsuno, T., 1970. Vertical propagation of stationary planetary waves in the winter Northern Hemisphere. J. Atmos. Sci. 27, 871–883.

Pawson, S., Naujokat, B., 1999. The cold winters of the middle 1990s in the Northern Lower Stratosphere. J. Geophys. Res. 104, 14209–14222. http://dx.doi.org/10.1029/1999JD900211.

PennState, 2016. Chi-square Distribution Table (Accessed 20 March 2017). http://sites.stat.psu.edu/~mga/401/tables/Chi-square-table.pdf.

Pogoreltsev, A.I., Savenkova, E.N., Pertsev, N.N., 2014. Sudden stratospheric warmings: the role of normal atmospheric modes. Geomag. Aeron. 54 (3), 357–372.

Pogoreltsev, A.I., Savenkova, E.N., Aniskina, O.G., Ermakova, T.S., Chen, W., Wei, K., 2015. Interannual and intraseasonal variability of stratospheric dynamics and stratosphere–troposphere coupling during northern winter. J. Atmos. Sol. Terr. Phys. 136, 187–200.

Quiroz, R., 1975. Stratospheric evolution of sudden warmings in 1969-74 determined from measured infrared radiation-fields. J. Atmos. Sci. 32, 211–224. http://dx.doi.org/10.1175/1520-0469(1975)032<0211:TSEOSW>2.0.CO;2.

Reichler, T., Kim, J., Manzini, E., Kröger, J., 2012. A stratospheric connection to Atlantic climate variability. Nat. Geosci. 5, 783–787. http://dx.doi.org/10.1038/ngeo1586.

Rice, J.A., 2006. Mathematical Statistics and Data Analysis, third ed. Duxbury Press, Belmont.

Rienecker, M.M., Suarez, M.J., Gelaro, R., et al., 2011. MERRA: NASA's Modern-era retrospective analysis for research and applications. J. Clim. 24, 3624–3648. http://dx.doi.org/10.1175/JCLI-D-11-00015.1.2011.

Robinson, W.A., 1985. A model of the wave 1 – wave 2 vacillation in the winter stratosphere. J. Atmos. Sci. 41 (21), 2289–2304.

Scherhag, R., 1952. Die explosionsartigen Stratosparenerwarmungen des Spatwinters 1952. Ber. Det. Wetterd. U. S. Zone 38, 51–63.

Schoeberl, M., 1978. Stratospheric warmings- observations and theory. Rev. Geophys. 16, 521–538. http://dx.doi.org/10.1029/RG016i004p00521.

Schoeberl, M., Hartmann, D., 1991. The dynamics of the stratospheric Polar Vortex and its relation to springtime ozone depletions. Science 251, 46–52. http://dx.doi.org/10.1126/science.251.4989.46.

Siskind, D.E., Eckermann, S.D., Coy, L., et al., 2007. On recent interannual variability of the Arctic winter mesosphere: implications for tracer descent. Geophys. Res. Lett. 34, L09806 http://dx.doi.org/10.1029/2007GL029293.

Swinbank, R., O'Neill, A., 1994. A stratosphere-troposphere data assimilation system. Mon. Weather Rev. 122, 686–702.

Thompson, D.W.J., Baldwin, M.P., Wallace, J.M., 2002. Stratospheric connection to northern Hemisphere wintertime weather: implications for prediction. J. Clim. 15, 1421–1428. http://dx.doi.org/10.1175/1520-0442(2002)015<1421:SCTNHW>2.0.CO;2.